

Transient Calcium Carbonate Hexahydrate (Ikaite) Nucleated and Stabilized in Confined Nano- and Picovolumes

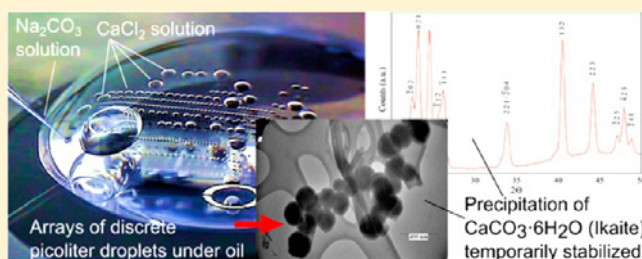
Isaac Rodríguez-Ruiz,^{†,‡} Stéphane Veessler,[‡] Jaime Gómez-Morales,^{*,†} José Manuel Delgado-López,[†] Olivier Grauby,[‡] Zoubida Hammadi,[‡] Nadine Candoni,[‡] and Juan Manuel García-Ruiz[†]

[†]Laboratorio de Estudios Cristalográficos, IACT (CSIC-UGR), Avda. de las Palmeras, 4, 18100 Armilla, Granada, Spain

[‡]CINaM-CNRS, Aix-Marseille Université, Campus de Luminy, F-13288 Marseille, France

S Supporting Information

ABSTRACT: Calcium carbonate precipitation at different values of the nominal ionic activity product (IAP) is studied in nanoliter and picoliter droplets at $(20 \pm 2)^\circ\text{C}$. Experiments are carried out through direct mixing of equimolar reactant solutions using two different setups: first, droplet-based microfluidics using Teflon capillaries (nanoliter experiments) and second, the microinjection technique under oil (picoliter droplets). Instantaneous precipitation of a metastable CaCO_3 phase is initially observed. This phase is stabilized in time by reducing the initial volume of the experiments from the nano- to picoliters range and when the $\text{CaCl}_2/\text{Na}_2\text{CO}_3$ ratio approaches 1. Further analysis by X-ray diffraction, transmission electron microscopy, and selected area electron diffraction confirms the first nucleated phase is $\text{CaCO}_3 \cdot 6\text{H}_2\text{O}$ (ikaite) and in few droplets ikaite plus $\text{CaCO}_3 \cdot \text{H}_2\text{O}$ (monohydrocalcite). No evidence of amorphous calcium carbonate (ACC) is found even in conditions where the IAP exceeds the solubility product of this phase. The *in vitro* finding of ikaite formation and stabilization due to volume confinement is an unexpected result since it is the first time that this hydrous phase is stabilized at room temperature (it is normally found at near 0°C) in the absence of additives. This result can be of interest for those biomineralization processes occurring in the confined volumes of intracellular vesicles and for biomimetic materials science in general.



1. INTRODUCTION

Nowadays the use of confinement in small volumes for preparing both inorganic and organic crystals is attracting increasing scientific and technological interest. Since the probability of observing the formation of a crystal during a nucleation process is very low due to its stochastic nature,¹ confinement in small droplets permits the location of nucleation events in space, and thus it makes their observation possible.^{1–4} Nucleation of calcium carbonate (CaCO_3) in small confined volumes is a widespread natural and environmental phenomenon. Thus, in many biomineralization processes, mineral is formed in compartmentalized well defined volumes such as intracellular vesicles⁵ and at relatively high supersaturations.^{6–8} In the conservation of cultural heritage, restoration of weathered carbonate stones in monuments and statuary can be carried out by bacterially induced calcium carbonate mineralization in small stone pores.⁹ In geological storage of CO_2 , precipitation of CaCO_3 is produced at high supersaturations by injecting pressurized CO_2 in the small pores and cracks of deep permeable geological formations. Here it reacts with earth alkali ions found in solution to form alkali earth carbonates and concretely with calcium ions to form CaCO_3 .¹⁰ In such a context, the precipitation of calcium carbonate may have an important impact on the permeability of the geological formation, as well as on its long-term storage capability. For these reasons, nucleation of CaCO_3 , and the

possible effects that confinement in small volumes exerts on it, is nowadays of increasing social and environmental interest.

Controlled-pore glasses, membranes, and other nanoporous materials have been reported to date as confining environments. These materials are generally in contact with the bulk solution, limiting the availability of reactants and generating the depletion of free molecules when the nucleation events take place.^{11–13} Microemulsions have also been used to produce confinement in droplets, in order to measure nucleation rate and critical nucleus size via a thermal method.^{14,15} Generation of small droplets^{1–4} offers the possibility of volume discretization and spatial confinement. It permits the control of nucleation events in a particular space that can be directly observed and monitored. To this end, regular arrays of microdroplets have been generated on patterned self-assembled monolayers as substrates to investigate the polymorphism of some organic compounds,^{3,16,17} reaching supersaturation through controlled evaporation of undersaturated droplets and finding access to different polymorphs by very high evaporation rates. Related to this work is the use of small droplets (or droplet-based methods) to study nucleation and polymorphism of calcium carbonate (CaCO_3) at low super-

Received: November 8, 2013

Revised: December 20, 2013

Published: January 16, 2014

saturations.^{18,19} CaCO_3 is one of the main compounds involved in the biomineralization and scaling process. It is also of great interest for its industrial applications as filler in plastics, rubber, paper, paints and pigments, and the food and pharmaceutical industry, in addition to the plastisol industry for car underbody paints, among many others.^{20–22} For both, natural and industrial processes, the control of either the calcium carbonate nucleating phase and/or its growth is essential for determining not only the necessary or desired polymorph, morphology, and size distribution of the crystals but also the subsequent properties of the natural (biomineral) or manufactured composite materials.

When CaCO_3 precipitates from highly supersaturated solutions in a batch process, it is known that amorphous metastable calcium carbonate (ACC) nucleates first and transforms to more stable phases according to the Ostwald's step rule.^{23,24} The initial formation of an ACC phase has been explained through both classical and nonclassical approaches. The classical approach assumes a lower nucleation barrier for amorphous than for crystalline phase, therefore kinetically favoring the formation of the metastable phase,²⁵ while the nonclassical one suggests that nucleation occurs through aggregation of prenucleation clusters.²⁶ Evidence of structural preformation and the nucleation of different ACC species which later transform into vaterite or calcite was found at different pH conditions.²⁶ In addition, it was shown that within narrow supersaturation conditions in which ACC solubility is not reached, it is possible for other hydrated metastable CaCO_3 phases to precipitate.²⁷ CaCO_3 hydrated crystalline phases are ikaite (IK, $\text{CaCO}_3 \cdot 6\text{H}_2\text{O}$) and monohydrocalcite (MHC, $\text{CaCO}_3 \cdot \text{H}_2\text{O}$). IK is known to precipitate steadily at low temperatures or high pressures.^{28,29} In nature and in the laboratory, the mineral readily crystallizes from solution at temperatures near 0 °C. At temperatures below 25 °C IK was obtained as a transient phase that rapidly transformed into vaterite and/or calcite, although it could be partially stabilized by using triphosphate.³⁰ On the other hand, the stability of MHC has long been debated.³¹ Generally, MHC is formed from ACC and transforms to calcite and/or aragonite,^{31–33} although it was found to be stable for centuries in natural ancient sediments.^{34,35}

This paper presents experiments performed in additive-free solutions at room temperature and medium to high values of the nominal ionic activity products in which ikaite (not ACC) is the first nucleating phase. The IK phase is stabilized in time by the effect of confinement and stoichiometric mixing ratio of the reactants. This finding can be relevant in the field of biomineralization and biomimetic materials science. Biomineral deposition in the confined volume of intracellular vesicles⁵ proceeds by the nucleation of an ACC as a disordered transient precursor that later transforms to the anhydrous calcite⁸ or by the coexistence of two ACC precursors, one hydrated (ACC- H_2O) and the other not.³⁶ The *in vitro* finding of IK formation due to volume confinement suggests that this phase might be explored as an alternative *in vivo* transient precursor for the formation of calcite biominerals. In parallel, IK by itself is proposed as an accessible CaCO_3 material at room temperature or as a transient precursor for the preparation of calcite- or vaterite-based biomimetic materials with tailored physicochemical and morphological properties.

2. EXPERIMENTAL SECTION

2.1. Reagents and Solutions. Sodium chloride (NaCl, ACS reagent, $\geq 99.0\%$ purity), calcium chloride dihydrate ($\text{CaCl}_2 \cdot 2\text{H}_2\text{O}$, Bioextra, $\geq 99.0\%$ purity), and sodium carbonate monohydrate ($\text{Na}_2\text{CO}_3 \cdot \text{H}_2\text{O}$, ACS reagent, 99.5% purity) were supplied by Sigma-Aldrich. FC-70 fluorinated oil and paraffin oil were supplied by Hampton Research. Ultrapure water (0.22 μS , 25 °C, Milli-Q, Millipore) was used to prepare all the solutions. Na_2CO_3 and CaCl_2 solutions of concentrations ranging from 10 to 200 mM were prepared by dilution of corresponding 1 M stock solutions and filtered by using 0.22 μm Millipore membranes. Ionic strength was adjusted by adding the necessary amount of NaCl (afterward solutions were refiltered). Speciation, nominal ion activity product (IAP) and saturation index (S.I. = $\log \text{IAP}/K_{\text{sp}}$) with respect to the calcite phase of solutions obtained by mixing equimolar volumes of Na_2CO_3 and CaCl_2 were determined by using PHREEQ-C software³⁷ considering chloride mean-salt ionic activity-coefficient data³⁸ in the Debye–Hückel equation and equilibration of all solutions with atmospheric CO_2 .

2.2. Droplet-Based Microfluidic Experiments (Nanololumes). Experiments in nanoliter droplets (2–3 nL) whose nominal IAPs range in the interval from 2.82×10^{-8} to $5.25 \times 10^{-6} \text{ mol}^2 \cdot \text{L}^{-2}$ (S.I. from 0.9 to 3.18), were performed in HPFA (Teflon polymer) capillaries of 150 μm internal diameter. Equimolar solution volumes of Na_2CO_3 and CaCl_2 were pumped through a PEEK T junction and mixed in a capillary (2.8 cm long). This capillary is connected to a second T-junction (for a more detailed description see refs 4 and 39), where the oil used as the carrier fluid (fluorinert oil FC-70) arrives to generate the droplets (see Figure S1a, in the Supporting Information). In each experiment, an array of nanoliter droplets was generated inside the Teflon capillary (as shown in Figure S1b). After the two reagent solutions were mixed, an initial precipitate was formed almost instantaneously in the capillary before the T-junction with oil. Then, this precipitate transformed to a more stable phase. We thus optimized the flow rates of both reagent solutions and oil in order to observe this transition within the generated droplets and not inside the capillary connecting the first T-junction. The total mixing flow rate for the experiments was 6 mL/h, representing a residence time of 0.5 s in the connecting capillary. Monitoring was carried out through direct observation with a Wild Heerbrugg M420 Makroskop and a Nikon Diaphot inverted microscope at room temperature (20 ± 2 °C). *In situ* observations were performed from the moment of mixing the initial solutions to the end of the experiments (which lasted from several hours to several days).

2.3. Microinjection Experiments (Picovolumes). Experiments in picoliter droplets (from 800 pL to 30 pL) with $\text{CaCl}_2/\text{Na}_2\text{CO}_3$ molar ratios between 0.25 and 3.0, whose IAPs range from 6.16×10^{-9} to $3.09 \times 10^{-7} \text{ mol}^2 \cdot \text{L}^{-2}$ (S.I. from 0.27 to 1.97), were carried out using a Femtojet microinjector (Eppendorf). Solutions were first introduced on different femtotips (Eppendorf) and then injected under a 30 μL droplet of paraffin oil. A schematic representation of the set up and images of the injection tip and droplet arrays are shown in Figure S2 in the Supporting Information. Arrays of picoliter droplets of CaCl_2 solutions were deposited over a plastic coverslip. Then, Na_2CO_3 equimolar picoliter droplets were added with a second tip to the first droplets in different volume ratios, thus generating droplet mixtures with different molar ratios, directly in a confined space. Afterward, water slowly diffuses from the crystallization droplets through the layer of paraffin oil, resulting in an increase of the IAP. Femtotips, attached to a capillary holder, were controlled by a homemade micro-manipulator consisting of three miniature translation stages MS30 (Mechonics AG) in X, Y, and Z with a displacement of 18 mm in the three directions by steps of 16 nm.⁴⁰ Experiments were monitored with a Zeiss Axio Observer D1 inverted microscope, and initial and mixed volumes were determined through image analysis of the microdroplets, following a model reported elsewhere.⁴¹ *In situ* observation of the precipitation process was carried out from the time of initial droplets mixture until complete crystallization of the droplets (which lasted from 15 to 24 h).

2.4. Characterization. Characterization: High resolution transmission electron microscopy (HRTEM) and selected area electron diffraction (SAED) experiments were performed with a JEOL 3010 instrument and a JEOL JEM-2010 both operating at 200 kV. The samples were prepared recovering the precipitates from the droplets under oil with the help of a capillary and depositing them over copper–carbon TEM grids lying on an adsorbent tissue. A droplet of hexane was immediately added over the grids to dissolve and remove the remaining mineral oil. SAED patterns analyses were performed by comparing measured distances and related measured angles among them with the help of CaRIne 3.1 crystallography software.⁴² d -spacings were assigned to their corresponding reflections under the criteria of the best fit with respect to reported d -spacings and related angles for calcium carbonate phases, that is, IK (Crystallography Open Database, COD, ID: 9008306, monoclinic), MHC (COD ID: 9010479, trigonal), aragonite (COD ID: 9000229, orthorhombic), vaterite (COD ID: 9007475, hexagonal), and calcite (COD ID: 9009667, trigonal). Field emission scanning electron microscopy (FESEM) and energy-dispersive X-ray spectroscopy (EDS) analyses were performed with a JEOL 6320F over the same grids after HRTEM analysis but coating them with a carbon thin film.

X-ray diffraction (XRD) patterns of precipitates obtained in nanoliters droplets were collected on a Mar Research single crystal rotating anode diffractometer (Cu $K\alpha$, $\lambda = 1.5418 \text{ \AA}$) equipped with a mar345 Image plate detector. Precipitates were fished from the droplets with the help of a nylon loop. XRD patterns of precipitates were collected in different images with an exposition time of 60 s/image, in a total rotating angle of 360° . Additionally, XRD patterns of precipitates obtained in picoliter droplets (microinjection experiments) were collected on a Bruker D8 Venture single crystal diffractometer equipped with a high brilliance incoatec micro source (Cu $K\alpha$, $\lambda = 1.5418 \text{ \AA}$) and a Photon100 detector at $2\theta = 0, 10, 20,$ and 30° . The frames were added and integrated with the Bruker APEX2 suite and the help of XRD2EVAL plug-in.

A Mach–Zehnder interferometer was used to characterize the mixing of droplets containing the reactant solutions. The experiment was performed in a Hele–Shaw⁴³ type cell composed by two parallel glass plates separated by a $200 \mu\text{m}$ gap. A laser diode beam (20 mW, 633 nm) was first passed through a Faraday isolator, so as to avoid any back-reflection toward the semiconductor laser cavity. A movable short focal length lens and a rotating ground glass diffuser allowed tuning the spatial coherence of the beam. The beam was subsequently divided in the reference and the sample (test) beams by means of a beamsplitter. The sample beam propagated through the experimental volume before being recombined with the reference beam. The result of the recombination is the generation of interference fringes (interferogram) at the imaging plane. The interferogram carries the information of the variation of the optical path between the object and the reference beam. A laser diode controller, CCD, and a temperature sensor for gathering the room temperature during the experiments were all controlled by means of Labview based scripts developed ad hoc for the application. For a qualitative description of the mixing, the concentration profiles for Ca^{2+} and CO_3^{2-} ions were simulated for the first instants of mixing, in a first approach, applying Fick's Law of diffusion.⁴⁴ For diffusion coefficient calculations, ionic radii of 0.99 \AA and 1.73 \AA were respectively considered for Ca^{2+} and CO_3^{2-} ions.⁴⁵

3. RESULTS

3.1. Calcium Carbonate Precipitation in Nanoliter Droplets (Microfluidic Setup). **3.1.1. Optical Microscopy Monitoring.** A sol composed of ultrafine particles describing Brownian motion was detected in all nanoliter droplets since the very beginning irrespective of their nominal IAP. The precipitates showed birefringence under crossed polarizers, increasing in intensity during the first minutes. This precipitation occurred instantaneously, just after the reactant solutions in the capillary were mixed. Subsequently, in most of the observed droplets ($\sim 95\%$ of the total), few calcite crystals

appeared while the first precipitate dissolved. The period of this transition was increased from a few minutes to several hours as the initial S.I. decreased from 3.18 to 0.9. To illustrate the precipitation process, Figure S3a,b is presented in the Supporting Information. In few droplets ($\sim 5\%$ of the total), in addition to the faceted calcite crystals, polycrystalline spherulitic aggregates of different sizes, morphologically assigned to vaterite, were also found.

3.1.2. Identification of the Precipitates. SEM micrographs of precipitates withdrawn after the first minutes show hollow hemispheres formed at the solution–oil interface by aggregation of $\sim 200 \text{ nm}$ spherulites (Figure 1a,b) as well as few calcite crystals displaying the typical (104) and (110) faces. EDS analysis of hemispheres confirms they contain Ca.

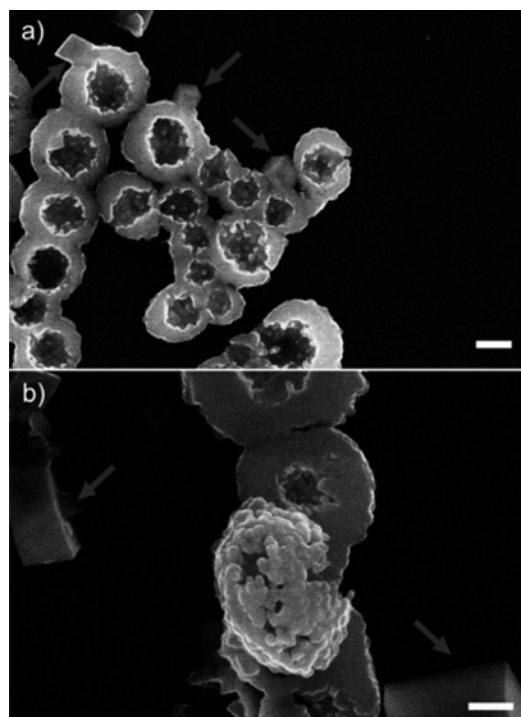


Figure 1. (a, b) SEM micrographs of precipitates obtained after the first minutes in a 3 nL droplet containing 50 mM CaCl_2 and 50 mM Na_2CO_3 (nominal IAP $5.25 \times 10^{-6} \text{ mol}^2 \cdot \text{L}^{-2}$, S.I. = 3.18). Micrographs show hollow hemispheres ($1\text{--}3 \mu\text{m}$) composed of 200 nm spherulites (panel b) and rhombohedral calcite (arrows). Scale bars = $1 \mu\text{m}$.

Moreover, HRTEM images over similar spherulites (Figure 2) identified a d -spacing of 2.54 \AA corresponding to the $(\bar{2} 2 3)$ ikaite crystallographic plane. For precipitates obtained in an array of identical nanoliter droplets (IAP $5.25 \times 10^{-6} \text{ mol}^2 \cdot \text{L}^{-2}$, S.I. = 3.18), the collected XRD patterns were analyzed and d -spacings were measured and assigned to different phases. The data are presented in Table S1 of the Supporting Information. It is noteworthy that the presence of vaterite is negligible, as confirmed by SEM and optical microscopy observations.^{46,47} Additionally, no morphological evidence of the presence of aragonite was found by optical or SEM microscopies,^{46,47} so both phases were not considered for the assignment. We clearly identified the (0 0 6) calcite plane, the (2 1 1) $\text{CaCO}_3 \cdot \text{H}_2\text{O}$ (MHC) plane, and the $(\bar{3} 1 2)$ $\text{CaCO}_3 \cdot 6\text{H}_2\text{O}$ (IK) plane. Other reflections were also found but are shared by more than one calcium carbonate phase (see Table S1 of the Supporting Information). Finally, for experiments lasting more than 30

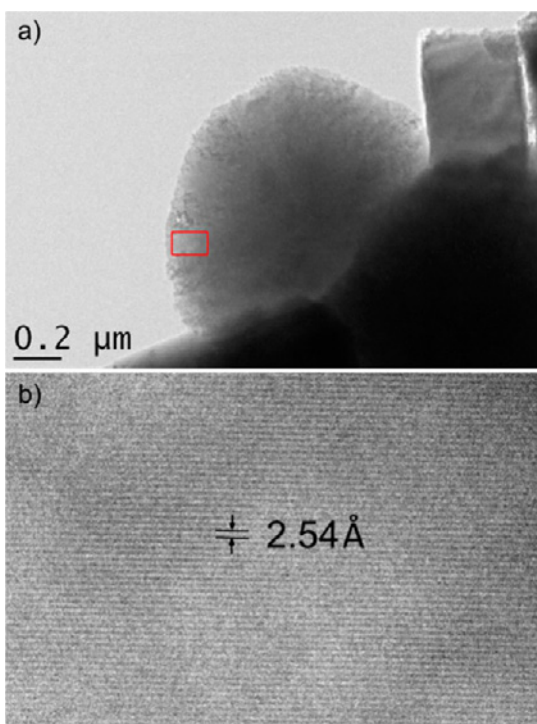


Figure 2. (a) TEM image of a precipitate collected few minutes after starting the experiment in a 3 nL droplet containing 50 mM CaCl_2 and 50 mM Na_2CO_3 (nominal IAP $5.25 \times 10^{-6} \text{ mol}^2 \cdot \text{L}^{-2}$, S.I. = 3.18). (b) Zoom of the spherulitic particle and measured d -spacing (2.54 Å corresponding to $(\bar{2} \ 2 \ 3)$ ikaite crystallographic plane).

days, XRD patterns of the precipitates revealed the presence of calcite only.

3.2. Calcium Carbonate Precipitation in Picoliter Droplets (Microinjector Setup). **3.2.1. Optical Microscopy Monitoring.** We found the following results: first, in all droplets, irrespective of the initial nominal IAP, the nucleation of thousands of ultrafine particles undergoing Brownian motions (a viscous sol) occurred during the first few minutes of the experiment (Figure 3a–d). This precipitate remained stable in many of the droplets until their complete evaporation ($\sim 2/3$ from a total of ~ 120 experiments). Second, in $\sim 1/3$ of the droplets precipitates were stable for several minutes/hours until the appearance of few rhombohedral calcite crystals (or vaterite in a few droplets at the lowest IAPs). These phases grew by forming around a radial area of depletion of the first precipitate (Figure 3e–h), thus suggesting a solvent-mediated phase transition (SMPT), as previously reported.⁴⁸ Third, once the second and more stable phase appeared, the sol completely disappeared in a short period, from a few seconds to a few minutes. No direct relationship between time to complete the phase transition and initial nominal IAP was observed, but the $\text{CaCl}_2/\text{Na}_2\text{CO}_3$ ratio has an effect. It is observed, in general, that longer transition periods occur for mixing ratios closer to 1. This is related to the number of crystals per droplet (Figure 4c): the lower the crystals number, the longer the phase transition.

For instance, we observed a lower tendency for the transformation of precipitate at a molar ratio of 1 (in 24 of 38 experiments first precipitate do not transform (Figure 4a)), whereas a higher tendency is observed for a molar ratio of 0.5 (in 31 of 43 experiments precipitate transforms (Figure 4b)).

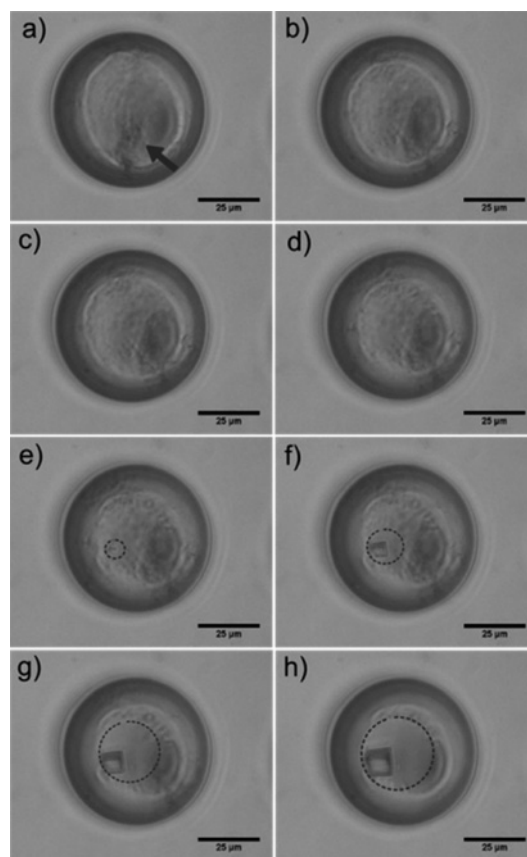


Figure 3. Time sequence of micrographs showing the course of precipitation in a 400 pL droplet containing 100 mM CaCl_2 and 100 mM Na_2CO_3 (nominal IAP = $3.16 \times 10^{-7} \text{ mol}^2 \cdot \text{L}^{-2}$, S.I. 1.98): (a) $t = 0$ s, a viscous sol is first formed (arrow); (b) $t = 10$ min; (c) $t = 20$ min; (d) $t = 80$ min; (e) $t = 112$ min, a calcite crystal nucleates; (f) $t = 115$ min, the depletion area surrounding the crystal starts to increase; (g) $t = 118$ min, growth of calcite crystal consumes most of the solute coming from the dissolution of the fine particles composing the sol; (h) $t = 120$ min, the growth of calcite stops few seconds after complete dissolution of the sol particles.

These observations indicate lower nucleation frequencies of the stable phase for a molar ratio of 1 than for a molar ratio of 0.5.

In order to confirm that the stability of the first precipitated sol is related to the absence of nucleation of a stable phase (and not to an unlikely inhibition of the precipitate dissolution), calcite single crystals were seeded in droplets with a micropipet where the sol remained stable for several hours. Micrographs of the process are shown in Figure 5. Once the crystal gets in contact with the solution inside the droplet, dissolution of the precipitate and growth of the calcite crystal take place concomitantly generating a depletion area surrounding the crystal (Figure 5c–e). Finally, the particles composing the sol completely dissolved (Figure 5f).

3.2.2. Characterization of Solution. With a view to understand the mixing process, Mach–Zehnder interferometric experiments were performed in $2 \mu\text{L}$ droplets. No clear interferences were observed in experiments performed by mixing CaCl_2 and Na_2CO_3 solutions due to their similar density. Nevertheless, a clear mixing front, generating a small interference (depicted in Figure 6a - 1 s by arrows) was drawn at the interface generated between the two reactant solutions due to precipitation of a CaCO_3 metastable phase. This front, clearly defined by the opacity of the first precipitate, appeared

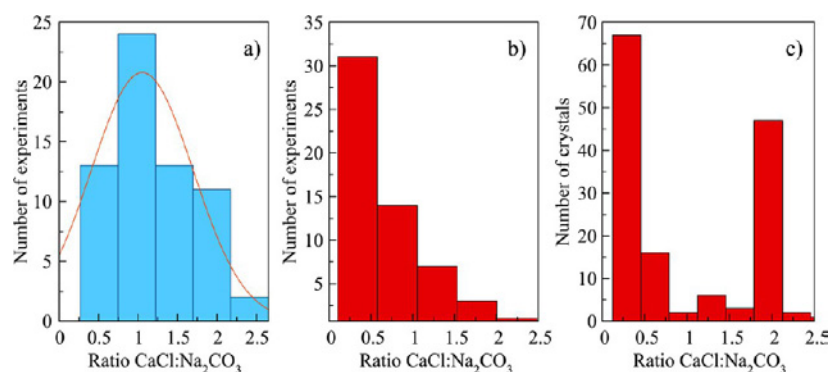


Figure 4. For the same molar ratio, the Y-axis represents: (a) number of experiments (droplets) where the first precipitate remained stable (two-thirds of the total) and Gaussian fitting of the distribution centered at a molar ratio of 1.053 ± 0.096 ; (b) number of experiments (droplets) in which a phase transition is observed (one-third of the total); (c) average number of crystals precipitated after the phase transition in each experiment (droplet). No significant number of experiments were performed at molar ratios higher than 2.0.

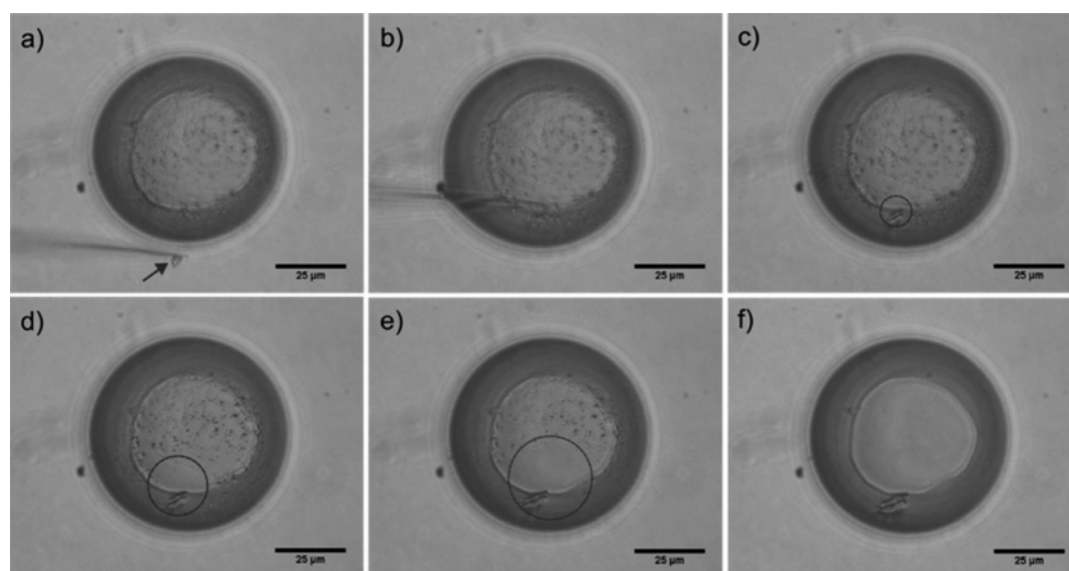


Figure 5. Micrographs represent a time sequence showing the dissolution of the first precipitate and the growth of a calcite seed. A calcite single crystal, marked with a black arrow in image (a), was seeded in the droplet with a micropipet, as shown in (b). Subsequently, dissolution of the precipitate and growth of the calcite crystal take place concomitantly generating a depletion area surrounding the crystal, as shown in panels (c–f). The droplet contained 20 mM CaCl_2 and 20 mM Na_2CO_3 solution. The whole sequence lasted 5 min.

spontaneously and subsequently disappeared when the metastable precipitate completely transformed into the more stable phase, while the density of this phase increased forming a cloud around the interface (depicted by an oval in Figure 6a–25 min and also present in the subsequent frames).

As the diffusivities of both reactants in water are similar, a supersaturation gradient is formed symmetrically around the mixing front in both directions generating, as a result, the nucleation of a metastable phase in the mentioned mixing front, where local supersaturation is maximum, as well as crystals of the stable phase (characterized by optical microscopy as calcite). It is worth noting that nucleation is taking place at the interface of the two solutions, therefore at a higher IAP than the nominal one calculated for an ideal mixing of the two reactants. This initial IAP value is very close to the one given by the sum of reactant concentrations of the two droplets. For a qualitative description, Figure 6b depicts simulated concentration profiles of Ca^{2+} and CO_3^{2-} ions during first instants of mixing. It can be appreciated that for a mixing time of only 10 ms the concentration in the mixing front (around $\pm 1 \mu\text{m}$

thickness) is 90% of the initial ion concentration of each droplet. To illustrate the diffusive regime of the mixing, two solutions of different densities were mixed to obtain clear interferometric bands. A sequence of frames is shown in Figure S4 of the Supporting Information. A higher number of interferometric bands along the mixing interface during the first moments (Figure S4) reveal a maximum concentration gradient and a diffusion of the more concentrated droplet to the less concentrated one.

3.2.3. Identification of the Precipitates. XRD patterns collected from initial precipitates after mixing the reactant solutions in $\sim 200 \text{ pL}$ droplets with S.I. ≈ 1.4 are shown in Figure 7. Figure 7d shows in green a diffractogram collected at room temperature in which $20\frac{2}{3}11$ and $\bar{3}15\text{IK}$ reflections (PDF card file 370416) are well observed. Particles from three different experiments were independently diffracted showing the same diffractogram. To increase the number of reflections by diffracting a higher number of particles, whole droplets were fished from underneath the oil and instantaneously quenched to 100 K under N_2 . This prevented the droplets from slipping

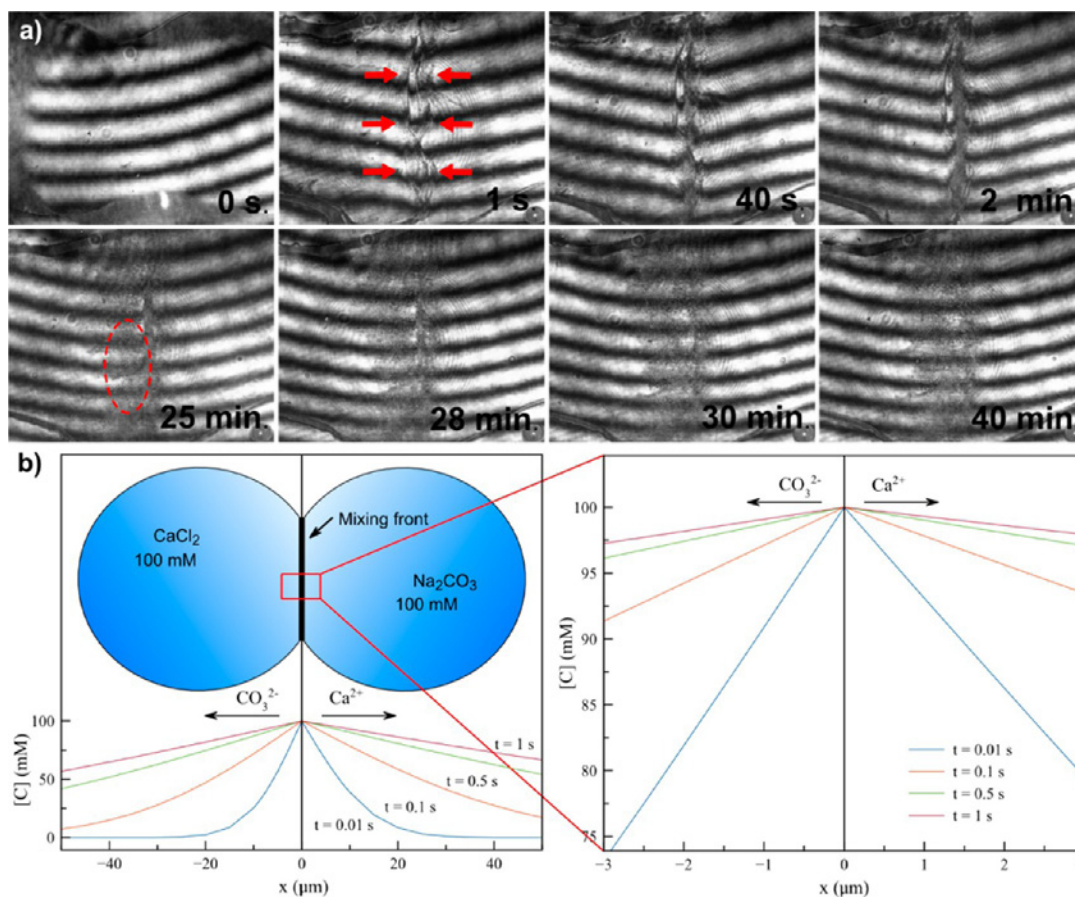


Figure 6. (a) Series of eight frames selected from the interferometric experiment (time scale, 7 frames/s) corresponding to the mixing of a 1 μL droplet 100 mM CaCl_2 with a 1 μL droplet 100 mM Na_2CO_3 ; (b) simulation of concentration profiles for Ca^{2+} and CO_3^{2-} ions corresponding to the mixing of micrometer-sized droplets with the same concentration of experiments in panel a. $x = 0$ is considered as an infinite source of reactants from each side, in order to simplify the calculations.

down when locating them vertically in the diffractometer and prevented their fast evaporation. Samples were also recovered from three other independent experiments, immediately quenched and placed on the diffractometer, and showed similar patterns among them. Diffractograms are shown and compared in Figure 7, panel a (red), b (purple), and c (blue) in order to provide a higher number of reflections. An important number of the characteristic IK reflections are displayed in the patterns (PDF card file 370416). However, it is noteworthy that XRD experiments were performed over a small number of particles, and, therefore, it is not possible to observe the reflections corresponding to all the crystallographic planes of IK, as not all of them were found in diffraction conditions.

HRTEM analyses of first precipitates in picoliter droplets show the presence of a crystalline CaCO_3 phase displaying similar spherulitic morphology and size to those particles found in the experiments performed in nanoliter droplets. These particles collapse under the electron beam when high energy electrons are applied (200 keV) and transform to a polycrystalline particle. This transformation has been found to happen with other materials and is explained by the loss of structural H_2O molecules due to the energy applied.⁴⁹ Figure 8 shows the transformation of two of these particles under the electron beam and the corresponding SAED patterns, before and after a short period under the electron beam. To better show this phenomenon, Figure 8a shows a time sequence for the transformation of a crystalline particle close to a calcite crystal,

which remains stable under the electron beam. SAED analyses (Figure 8b,c) are also in agreement with our previous experiments of samples from nanoliter experiments, revealing the presence of IK. In addition, more images of spherulitic particles are shown in Figure S5 of the Supporting Information confirming the presence of IK. It is worth noting that SAED patterns are not perfectly oriented, as the intensity of equivalent spots is not the same. Since the lifetime of the crystallite under the beam is very short, this does not allow us to reorient the sample before the crystallite is completely transformed.

4. DISCUSSION

In this paper, the effects of confinement on the nucleation of calcium carbonate in the volume range from nanoliters to picoliters (droplets radius from around 100 to 20 μm) with two different set ups for droplet generation were studied. The $\text{CaCl}_2/\text{Na}_2\text{CO}_3$ ratio of the mixed droplets is controlled by changing the ratio of the volumes of the two reactant droplets in the picoliter setup. In each set up, the micromixing processes exerts a crucial role in how supersaturation is generated. Indeed, by using the nanoliter microfluidic set up, micromixing can be seen to take place at the contact between two solutions flowing in a laminar regime, while in the picoliter microinjector setup micromixing takes place by diffusion of the reagents through the mixing plane. In both cases, at the contact plane the local IAP is higher than the nominal one, and as a

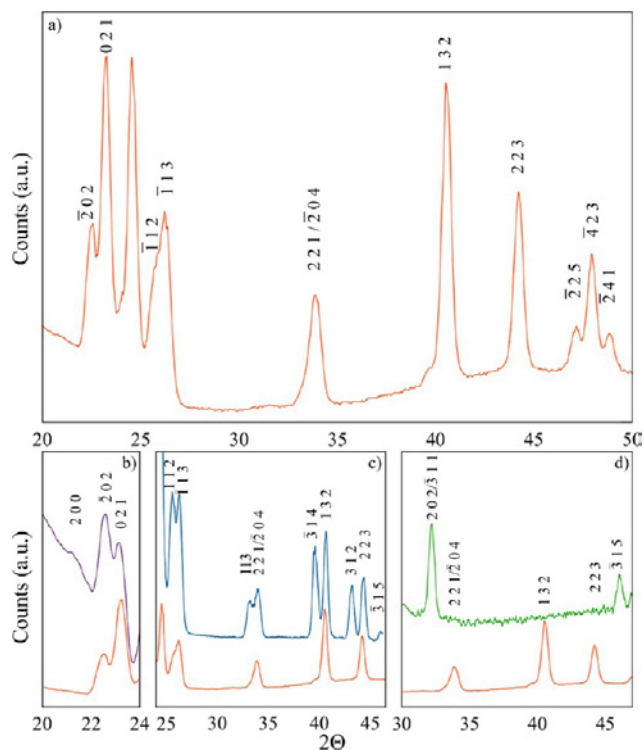


Figure 7. XRD diffractograms collected from precipitates obtained just after mixing reactants in ~ 200 pL droplets (S.I. ≈ 1.4). All the peaks correspond to IK reflections (PDF card file 370416). The red line in (a–d) shows the same diffractogram. Panels b, c, and d are an enlarged view of the red diffractogram (a), compared with other three different XRD diffractograms, in different colors, in which other reflections appear providing complementary information.

consequence the K_s of the metastable phase is overtaken (supersaturation is generated), leading to its precipitation.

The characterization by SAED and XRD confirms that the formed precipitate consist of crystalline hydrated forms of CaCO_3 such as IK and in few cases MHC. Moreover, no evidence of the initial precipitation of ACC was found. The hydrated phase remains stable for different periods of time: in most of the picoliter droplets it remains stable until complete droplet evaporation. However for some droplets, the stabilization time depends on the initial $\text{CaCl}_2/\text{Na}_2\text{CO}_3$ ratio, becoming maximal as this ratio approaches 1. Afterward, calcite (sometimes vaterite) nucleates and grows at the expense of the hydrated phase. This SMPT process leads to one or two calcite crystals at a molar ratio of 1.

The nucleation and stabilization of the first metastable phase seems to be promoted by the combined effect of three parameters which has been previously studied. These are (high) supersaturation,^{3,16,50,51} stoichiometry,^{52–58} and (reduction of) volume.^{59,60} These three aspects are considered and discussed below

4.1. Effect of Mixing of Reactants Solutions on Nucleation of Metastable Phases. XRD and SAED experiments confirm the SMPT process (Figures 3 and 5). Nucleation of the metastable phase occurs followed by nucleation of the stable phase and its growth at the expense of the dissolution of the first precipitate. Thus, as no calcite reflections were detected in the XRD experiments, the first precipitation of nanocrystals of calcite undergoing ripening can be ruled out. In addition, the experiment presented in Figure 5 confirms that metastability can be broken by seeding with a more stable phase. The metastable phase has been identified as a hydrated phase, IK and in few cases MHC. Thus, the solution has to be supersaturated with respect to at least MHC ($\text{IAP} > K_{s(\text{MHC})}$). It is noteworthy that when $\text{IAP} < K_{s(\text{MHC})}$, the

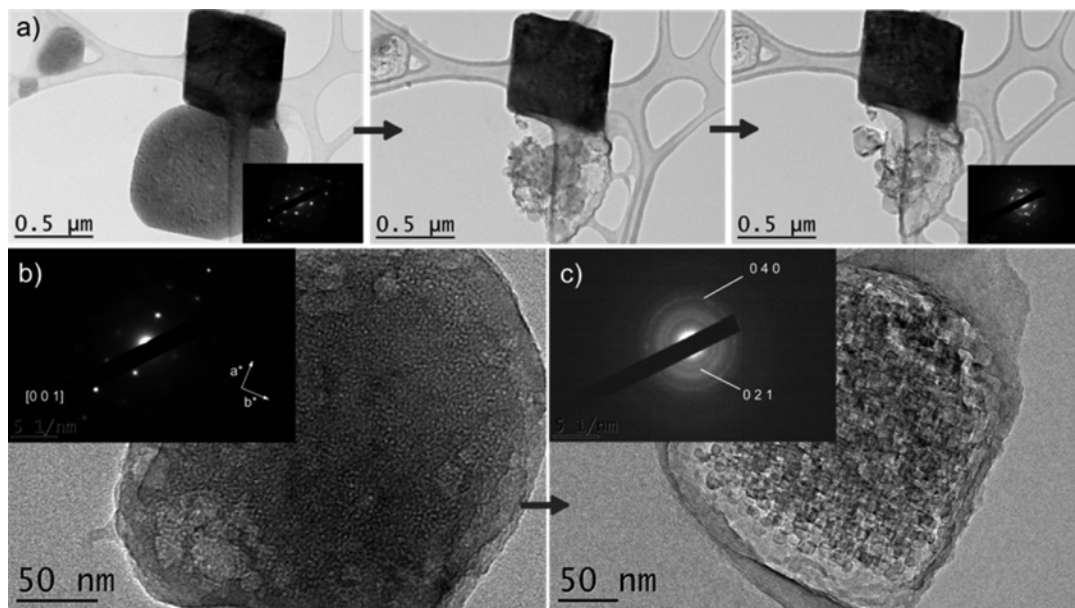


Figure 8. (a) Transformation sequence of a crystalline particle under the electron beam and close to a faceted calcite crystal which remain unaltered. (b, c) Transformation of a crystalline particle under the electron beam and collected SAED patterns at the first instants of the experiments and during its transformation. The pattern in the first instants is collected along the $[0\ 0\ 1]$ direction, showing the orientation of axis a^* and b^* in the reciprocal lattice, corresponding to the lattice parameters of IK ($a = 8.79$ Å, $b = 8.31$ Å, $c = 11.02$ Å, $\alpha = 90^\circ$, $\beta = 110.5^\circ$, $\gamma = 90^\circ$). SAED pattern in (c) is representative of a polycrystalline material, due to the decomposition of the single crystal into smaller crystallites, under the electron beam. Measured d -spacings correspond to 0 4 0 and 0 2 1 ikaite reflections, equal to 2.06 Å and 3.82 Å respectively.

solution remains metastable and the precipitation does not occur instantaneously.²⁷ However, as soon as the IAP overtakes the $K_{s(\text{MHC})}$ nucleation occurs spontaneously. Nonetheless, in most of the experiments performed, spontaneous nucleation has been observed (Figure 3), despite the initial nominal IAP < $K_{s(\text{MHC})}$. IAP is calculated for an ideal homogeneous reactant solution; that is to say, mixing is considered instantaneous. However, as it has been demonstrated (Figure 6), the mixture of the reactant solutions is not instantaneous, and therefore, the chemical conditions in a microliter-sized droplet cannot be considered homogeneous.⁶¹ For the microfluidic experiments in Teflon capillaries, the mixing occurs through a micrometer-sized channel in which laminar flow generates a diffusive interface between reactant solutions, in the absence of convective forces.^{2,62} On the other hand, in microinjection experiments, mixing takes place when two micrometer-sized droplets containing the reagents come into contact, generating an instantaneous nucleation front, corresponding to the first contact interface between both droplets, and later homogenizing by diffusion, as confirmed by interferometric experiments (Figure 6 and Figure S4, Supporting Information). The formation of local supersaturation maxima in the mixing front of the solutions explains why nucleation of an hydrated phase occurred when nominal IAP < $K_{s(\text{MHC})}$ but the local IAP > $K_{s(\text{MHC})}$. For the same reasons, we found crystals with rounded or lobulated morphologies, corresponding to the vaterite phase, for some droplets where the nominal IAP < K_s for vaterite ($1.336 \times 10^{-8} \text{ mol}^2 \cdot \text{L}^{-2}$). This occurred in 11 out of 18 experiments after the dissolution of the first precipitated metastable phase. To further illustrate these findings, Figure 9 shows the initial nominal IAP values as a function of the mixing $\text{CaCl}_2/\text{Na}_2\text{CO}_3$ ratio (Figure 9a) for all droplets generated by microinjection in the picoliter range (from 800 to 30 pL) and the initial IAP calculated in the mixing front at $t = 0$ for the different reactant concentrations. This IAP overcomes $K_{s(\text{MHC})}$ for most of the microinjection experiments.

4.2. Ikaite as a Transient Precursor Phase. The phase diagram of CaCO_3 is rich. Starting from the least stable phase to the most stable one, it is composed of ACC, IK, MHC, vaterite, aragonite, and calcite. The solid characterization has provided evidence for three phases IK or MHC and in some experiments calcite (and in few cases vaterite) at the end (Figure 3). If the first phase to nucleate is metastable, in agreement with the Ostwald's step rule, the final concentration corresponds to the solubility of this phase, but the solution is still supersaturated for more stable phases to nucleate and for SMPT to proceed (growth of the stable phase at the expense of the metastable phase). Hereafter, we discuss the possible nucleation of metastable phases. First, if ACC has nucleated, and as no traces of ACC were detected in the first instants, ACC transformation to a more stable (but yet metastable) phase would happen fast. Second, the second metastable CaCO_3 phase is IK, known to nucleate at low temperatures and high pressures. It generally transforms to calcite while losing its water molecules, but it has also been reported to transform to MHC during its dehydration.⁶³ Third, MHC is the next metastable hydrated CaCO_3 phase, and its stability has long been debated.³¹ Laboratory studies indicate that MHC is formed from ACC and transforms to aragonite or calcite in solution within several days.^{31–33}

However, observations in nature demonstrate that MHC has been preserved in ancient sediments formed more than a thousand years ago.^{34,35} Water temperature does not seem to

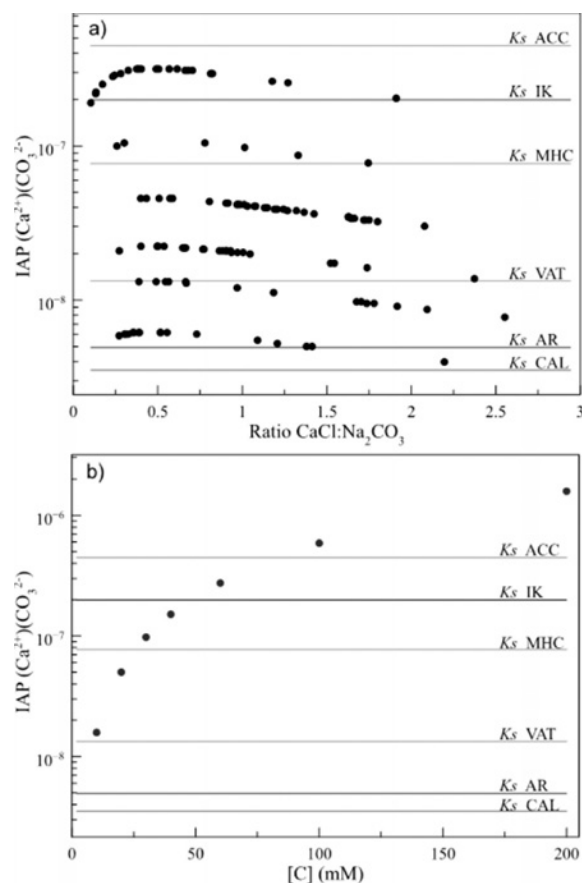


Figure 9. (a) Plot of the estimated nominal IAP ($\text{mol}^2 \cdot \text{L}^{-2}$) vs molar ratio of reagent solutions for the whole experimental data set used in microinjection experiments. (b) Plot of the IAP in the mixing front of solution (calculated at mixing time $t = 0$) vs initial reagent concentration. IAP values estimated by PHREEQC.³⁷ Solubility product constants (K_s , $\text{mol}^2 \cdot \text{L}^{-2}$) for all calcium carbonate phases were calculated at 20 °C using equations reported by Elfil et al.²⁷

be an important factor for MHC formation, and its solubility is higher than those of calcite, aragonite, and vaterite but lower than those of IK and ACC at ambient temperature. MHC phase transition has been reported to be solvent mediated where the nucleation and growth of the stable crystalline phase are the rate-limiting steps of the transformation.⁶⁴ We rule out ACC nucleation (at least for the moment), as no traces of ACC were detected in the first instants. Thus, and due to the evidence for its presence in our experiments, IK may be proposed to be the first metastable phase to nucleate. Presence of MHC would be explained both by IK transformation or by MHC direct nucleation in the case of experiments at lower initial supersaturations.

A second point to discuss is the SMPT. This process requires the nucleation of a more stable phase than the hydrated phases. It can be vaterite, aragonite, or calcite. When SMPT occurred, it is always calcite (and in some cases vaterite) that is finally obtained. We know from the literature that it takes several hours for the transformation from vaterite to calcite in solution⁶⁵ and several months for that of aragonite to calcite⁶⁶ to be completed at room temperature. The possible effect of Na^+ and Cl^- ions, present in the solutions of our experiments, on this transformation has also been studied and discussed.⁶⁷ It was shown that the halide anions and most of alkali ions (including Na^+) do not affect the transformation rate. Hence,

the hypothesis of a first transition from a hydrated form to vaterite or aragonite and later a second transformation to calcite is to be ruled out. Thus, the transformation should take place from a first instantaneously precipitated hydrated calcium carbonate phase, IK or MHC to calcite. IK is not known to be formed biologically;⁸ however, the present results of IK nucleation as a stable transient precursor in confinement indicate that this possibility might not be so easily dismissed.

4.3. Effect of Volume in the Nucleation and Stabilization of Precipitates. The fact that experiments performed in nanoliter volumes and at a 1:1 molar ratio mostly showed a phase transition, while the first precipitate has been found to remain stable for longer periods at the picoliter scale, on equivalent injection experiments, indicates that volume reduction up to picoliter droplets exerts an effect of stabilization in the first nucleating phase. This is to say confinement stabilizes supersaturated solutions.⁶⁰ This effect has previously been observed for other metastable CaCO_3 phases. Indeed, it was observed for ACC to be stabilized in confinement at micrometer-scale separations,⁵⁹ and picoliter droplets in our experiments exert the same confinement effect.¹ It is known that higher supersaturations increase the probability of nucleating a metastable phase⁵¹ and that confinement can stabilize a metastable phase.¹⁶ Because the nucleated crystal(s) of the metastable phase decrease the supersaturation rapidly, the probability for a more stable nucleus to appear is reduced, and thus the SMPT process is postponed.⁶⁸ According to the classical theory of nucleation (CNT), nucleation frequency is directly related to the volume of solution. By reducing the volume, the probability of a nucleation event to occur is decreased. This phenomenon has been observed for a long time in microfluidic experiments and for many different substances.⁶⁹ A reduction in the reactive species to support the growing precipitates, together with the reduced probability for a stable cluster to nucleate and grow, explains the observations of mononucleation of a single calcite crystal, whose final size will be determined by the total amount of calcium and carbonate ions in the droplet.

Another effect related to the reduction of volume, which is the increase of pressure in the droplet, has been dismissed in our experiments. Indeed, by applying the Young–Laplace equation $\Delta P = 2\gamma/R$, which describes the equilibrium pressure difference sustained across the interface between two static fluids, ΔP being the excess of pressure inside the droplet due to its curvature, γ the surface tension of the solution in contact with the oil, and R the droplet radius, we can observe that for a representative droplet of our system, with $R = 25 \mu\text{m}$, and considering a γ value of 72 mN/m (water droplet in contact with air), ΔP is 0.057 atm. This extra pressure is not a significative amount to be considered the responsible factor for the stabilization of the IK phase. Only for sub-micrometer droplets ($R < 1 \mu\text{m}$) would the pressure be exerting an important effect.

4.4. Effect of Stoichiometry in the Stabilization of Precipitates. After the stability of the first precipitate for different molar ratios was analyzed, a very clear tendency was observed for the persistence of the metastable phase with time and the absence of any nucleation of the stable calcite phase for the experiments (given molar ratio of 1). In addition, the mononucleation of calcite is observed for those experiments that undergo the SMPT process where the molar ratios were also 1. As is described in Figure 4c, unstable precipitates at other different ratios displayed many calcite crystals after phase

transition. Many studies confirm that the solution stoichiometry of the reactant ions can affect the rate of calcite precipitation, although how it exactly affects this precipitation varies from publication to publication. An increase of the precipitation rate while decreasing the calcium to total carbonate ($\text{Ca}/\text{C}_\text{T}$) ratio was reported by Lin and Singer,⁵² whereas rate maxima at a molar ratio of 1^{53–55} and other particular stoichiometries^{56,57} have been also found. In our case, that is, the confined picoliter droplets and a stoichiometric molar ratio, a maximum nucleation rate of the metastable precipitate takes place, and thus this leads to the fastest consumption of reactant ions and therefore to a minimum remaining IAP but yet higher than K_s of calcite. At these conditions and according to CNT, few calcite nuclei (mononucleation) will form (indicating a low nucleation frequency), and the metastable phase will remain stable for longer periods. This explains the maximum number of stabilized experiments for the molar ratio of 1, as well as the symmetric behavior observed around this ratio. Indeed, the more the molar ratio differs from 1, the slower the nucleation rate (despite observing instantaneous precipitation) and the higher is the remaining supersaturation in the droplet and therefore the nucleation frequency for calcite, thus providing an environment that favors the nucleation of a higher number calcite crystals, as seen in Figure 4c.

5. CONCLUSIONS

Calcium carbonate precipitation at medium to high values of the nominal IAP has been studied in a confined volume, in nanoliter and picoliter droplets, at constant ionic strength and different molar ratios. Instantaneous precipitation of crystalline calcium carbonate hydrated phases has been confirmed by optical microscopy through birefringence under crossed polarizers, XRD and SAED. No evidence of ACC was found. Ikaite was found to be a transient metastable phase whose stability increased over time when reducing the volume of the droplets from nano- to picoliter range (in this case, until complete solvent evaporation) and for a stoichiometric molar ratio. In these later conditions, when a SMPT transformation was observed, nucleation of one or few calcite crystals (mononucleation) occurred. Precipitation of the hydrated metastable phase was observed at the interface of the two mixing droplets, where the supersaturation is higher than that after the complete mixing. Because of the location in space of the crystallization events in isolated volumes, confinement has been proven to be a good approach for the study of crystalline precipitation. Moreover, the mixing of reagent solutions by the microinjection technique has been demonstrated to provide a useful method for investigating the effect of confinement on precipitation. It has been shown that confinement exerts a clear effect in the temporary stabilization of IK in nano- and picovolumes at room temperature, as the nucleation and stabilization of this metastable phase has only been previously achieved by using low temperatures (near 0 °C), high pressures, or an additive (i.e., triphosphate).

■ ASSOCIATED CONTENT

Supporting Information

Figures S1–S5 and Table S1. This material is available free of charge via the Internet at <http://pubs.acs.org>.

■ AUTHOR INFORMATION

Corresponding Author

*E-mail: jaime@lec.csic.es.

Present Address

#Instituto de Microelectrónica de Barcelona, CNM-CSIC. Campus Universitat Autònoma de Barcelona (UAB). 08193 Cerdanyola del Vallès, Spain.

Notes

The authors declare no competing financial interest.

■ ACKNOWLEDGMENTS

This work was carried out within the framework of the Project MAT2011-28543 (Spanish MINECO). J.M.G.R., J.G.M., J.M.D.L, and I.R.R. belong to the research team “Factoría de Cristalización” (Consolider-Ingenio 2010) of the Spanish MINECO and Junta de Andalucía. The authors thank Damien Chaudansson and Serge Nietsche for HRTEM and SAED experiments and Luis David Patiño López for his valuable help with Mach–Zehnder interferometry experiments. I.R. also thanks the Consejo Superior de Investigaciones Científicas (CSIC) for his predoctoral JAE-Pre research contract and Dr. Frederic Harb for the fruitful discussions. We thank Dr. Marcus O’Mahony for English revision.

■ REFERENCES

- (1) Grossier, R.; Veessler, S. P. Reaching One Single and Stable Critical Cluster through Finite-Sized Systems. *Cryst. Growth Des.* **2009**, *9* (4), 1917–1922.
- (2) Bringer, M. R.; Gerdt, C. J.; Song, H.; Tice, J. D.; Ismagilov, R. F. Microfluidic systems for chemical kinetics that rely on chaotic mixing in droplets. *Philos. Trans. R. Soc. London, Ser. A* **2004**, *362* (1818), 1087–1104.
- (3) Lee, I.; Lee, A.; Myerson, A. Concomitant Polymorphism in Confined Environment. *Pharm. Res.* **2008**, *25* (4), 960–968.
- (4) Ildefonso, M.; Candoni, N.; Veessler, S. A Cheap, Easy Microfluidic Crystallization Device Ensuring Universal Solvent Compatibility. *Org. Process Res. Dev.* **2012**, *16* (4), 556–560.
- (5) Meldrum, F. C. Calcium carbonate in biomineralisation and biomimetic chemistry. *Int. Mater. Rev.* **2003**, *48* (3), 187–224.
- (6) Raz, S.; Testeniere, O.; Hecker, A.; Weiner, S.; Luquet, G. Stable amorphous calcium carbonate is the main component of the calcium storage structures of the crustacean *Orchestia cavimana*. *Biol. Bull.* **2002**, *203* (3), 269–274.
- (7) Nys, Y.; Hincke, M.; Hernandez-Hernandez, A.; Rodriguez-Navarro, A.; Gomez-Morales, J.; Jonchère, V.; Garcia-Ruiz, J.; Gautron, J. Structure, propriétés et minéralisation de la coquille de l’œuf: rôle de la matrice organique dans le contrôle de sa fabrication. *Inra Prod. Anim.* **2010**, *23* (2), 143–154.
- (8) Addadi, L.; Raz, S.; Weiner, S. Taking Advantage of Disorder: Amorphous Calcium Carbonate and Its Roles in Biomineralization. *Adv. Mater.* **2003**, *15* (12), 959–970.
- (9) Rodriguez-Navarro, C.; Rodriguez-Gallego, M.; Ben Chekroun, K.; Gonzalez-Munoz, M. T. Conservation of ornamental stone by *Myxococcus xanthus*-induced carbonate biomineralization. *Appl. Environ. Microbiol.* **2003**, *69* (4), 2182–2193.
- (10) Cailly, B.; Le Thiez, P.; Egermann, P.; Audibert, A.; Vidal-Gilbert, S.; Longaygue, X. Geological storage of CO₂: A state-of-the-art of injection processes and technologies. *Oil Gas Sci. Technol.* **2005**, *60* (3), 517–525.
- (11) Haller, W. Chromatography on glass of controlled pore size. *Nature* **1965**, *206* (4985), 693–696.
- (12) Jackson, C. L.; McKenna, G. B. The melting behavior of organic materials confined in porous solids. *J. Chem. Phys.* **1990**, *93* (12), 9002–9011.
- (13) Ha, J.-M.; Wolf, J. H.; Hillmyer, M. A.; Ward, M. D. Polymorph Selectivity under Nanoscopic Confinement. *J. Am. Chem. Soc.* **2004**, *126* (11), 3382–3383.
- (14) Liu, J.; Nicholson, C. E.; Cooper, S. J. Direct Measurement of Critical Nucleus Size in Confined Volumes. *Langmuir* **2007**, *23* (13), 7286–7292.
- (15) Kashchiev, D.; Clause, D.; Jolivet-Dalmazzone, C. Crystallization and critical supercooling of disperse liquids. *J. Colloid Interface Sci.* **1994**, *165* (1), 148–153.
- (16) Lee, A. Y.; Lee, I. S.; Myerson, A. S. Factors Affecting the Polymorphic Outcome of Glycine Crystals Constrained on Patterned Substrates. *Chem. Eng. Technol.* **2006**, *29* (2), 281–285.
- (17) Effenhauser, C. S.; Bruin, G. J. M.; Paulus, A.; Ehrat, M. Integrated Capillary Electrophoresis on Flexible Silicone Microdevices: Analysis of DNA Restriction Fragments and Detection of Single DNA Molecules on Microchips. *Anal. Chem.* **1997**, *69* (17), 3451–3457.
- (18) Stephens, C. J.; Kim, Y.-Y.; Evans, S. D.; Meldrum, F. C.; Christenson, H. K. Early Stages of Crystallization of Calcium Carbonate Revealed in Picoliter Droplets. *J. Am. Chem. Soc.* **2011**, *133* (14), 5210–5213.
- (19) Yashina, A.; Meldrum, F.; Demello, A. Calcium carbonate polymorph control using droplet-based microfluidics. *Biomicrofluidics* **2012**, *6* (2), 22001–22001-10.
- (20) Lowenstam, H. A.; Weiner, S. *On Biomineralization*; University Press: Oxford, 1989.
- (21) Hasson, D.; Avriel, M.; Resnick, W.; Rozenman, T.; Windreich, S. Mechanism of calcium carbonate scale deposition on heat-transfer surfaces. *Ind. Eng. Chem. Fundam.* **1968**, *7* (1), 59–65.
- (22) Garcia-Carmona, J.; Gomez-Morales, J.; Fraile-Sainz, J.; Rodriguez-Clemente, R. Morphological characteristics and aggregation of calcite crystals obtained by bubbling CO₂ through a Ca(OH)₂ suspension in the presence of additives. *Powder Technol.* **2003**, *130* (1–3), 307–315.
- (23) Ogino, T.; Suzuki, T.; Sawada, K. The formation and transformation mechanism of calcium carbonate in water. *Geochim. Cosmochim. Acta* **1987**, *51* (10), 2757–2767.
- (24) Bolze, J.; Peng, B.; Dingenouts, N.; Panine, P.; Narayanan, T.; Ballauff, M. Formation and Growth of Amorphous Colloidal CaCO₃ Precursor Particles as Detected by Time-Resolved SAXS. *Langmuir* **2002**, *18* (22), 8364–8369.
- (25) Navrotsky, A. Energetic clues to pathways to biomineralization: Precursors, clusters, and nanoparticles. *Proc. Natl. Acad. Sci. U.S.A.* **2004**, *101* (33), 12096–12101.
- (26) Gebauer, D.; Völkel, A.; Cölfen, H. Stable Prenucleation Calcium Carbonate Clusters. *Science* **2008**, *322* (5909), 1819–1822.
- (27) Elfil, H.; Roques, H. Role of hydrate phases of calcium carbonate on the scaling phenomenon. *Desalination* **2001**, *137* (1–3), 177–186.
- (28) Marland, G. The stability of CaCO₃·6H₂O (ikaite). *Geochim. Cosmochim. Acta* **1975**, *39* (1), 83–91.
- (29) Bischoff, J. L. The solubility and stabilization of ikaite (CaCO₃·6H₂O) from 0° to 25 °C: environmental and paleoclimatic implications for thynolite tufa. *J. Geol.* **1993**, *101* (1), 21–33.
- (30) Clarkson, J. R. Role of metastable phases in the spontaneous precipitation of calcium carbonate. *J. Chem. Soc. Faraday Trans.* **1992**, *88* (2), 243–249.
- (31) Taylor, G. F. The occurrence of monohydrocalcite in two small lakes in the south-east of South Australia. *Am. Mineral.* **1975**, *60* (7/8), 690–697.
- (32) Brooks, R.; Clark, L. M.; Thurston, E. F. Calcium Carbonate and Its Hydrates. *Philos. Trans. R. Soc. London, Ser. A* **1950**, *243* (861), 145–167.
- (33) Munemoto, T.; Fukushi, K. Transformation kinetics of monohydrocalcite to aragonite in aqueous solutions. *J. Mineral. Petrol. Sci.* **2008**, *103* (5), 345–349.
- (34) Abzaeva, A. A.; Bezrukova, E. V.; Bychinsky, V. A.; Fedenya, S. A.; Fukushi, K.; Gelety, V. F.; Goreglyad, A. V.; Ivanov, E. V.; Kalmychkov, G. V.; Kashiwaya, K.; Kawai, T.; Kerber, E. V.; Khomutova, M.Yu.; Khursevich, G. K.; Kim, J.-Y.; Krainov, M. A.;

- Kulagina, N. V.; Kuzmin, M. I.; Letunova, P. P.; Minourah, K.; Nahm, W.-H.; Narantsetseg, Ts.; Oyunchimeg, Ts.; Prokopenko, A. A.; Sakai, H.; Solotchina, E. P.; Tani, Y.; Tkachenko, L. L.; Tomurhuu, D.; Watanabeh, T. Sedimentary record from Lake Hovsgol, NW Mongolia: Results from the HDP-04 and HDP-06 drill cores. *Quat. Int.* **2009**, *205* (1–2), 21–37.
- (35) Stoffers, P.; Fischbeck, R. Monohydrocalcite in the sediments of Lake Kivu (East Africa). *Sedimentology* **1974**, *21* (1), 163–170.
- (36) Gong, Y. U. T.; Killian, C. E.; Olson, I. C.; Appathurai, N. P.; Amasino, A. L.; Martin, M. C.; Holt, L. J.; Wilt, F. H.; Gilbert, P. U. P. A. Phase transitions in biogenic amorphous calcium carbonate. *Proc. Natl. Acad. Sci. U.S.A.* **2012**, *109* (16), 6088–6093.
- (37) Parkhurst, D. L.; Appelo, C. A. J. *User's Guide to PHREEQC*; U.S. Geological Survey Water Resources Investigations Report; U.S. Geological Survey: Reston, VA, 1999.
- (38) Truesdell, A. H.; Jones, B. F. WATEQ, a computer program for calculating chemical equilibria in natural waters. *J. Res. U. S. Geol. Surv.* **1974**, *2*, 233–248.
- (39) Dombrowski, R. D.; Litster, J. D.; Wagner, N. J.; He, Y. Crystallization of alpha-lactose monohydrate in a drop-based microfluidic crystallizer. *Chem. Eng. Sci.* **2007**, *62* (17), 4802–4810.
- (40) Grossier, R.; Hammadi, Z.; Morin, R.; Magnaldo, A.; Veessler, S. Generating nanoliter to femtoliter microdroplets with ease. *Appl. Phys. Lett.* **2011**, *98* (9), No. 091916.
- (41) Rodríguez-Ruiz, I.; Hammadi, Z.; Grossier, R.; Gómez-Morales, J.; Veessler, S. Monitoring Picoliter Sessile Microdroplet Dynamics Shows That Size Does Not Matter. *Langmuir* **2013**, *29* (41), 12628–12632.
- (42) Boudias, C.; Monceau, D. *CaRIne Crystallography 3.1*; Senlis, France, 1989–1998.
- (43) Hele-Shaw, H. S. The flow of water. *Nature* **1898**, *58*, 33–36.
- (44) Fick, A. Ueber Diffusion. *Ann. Phys.* **1855**, *170* (1), 59–86.
- (45) Kester, D. R.; Pytkowicz, R. M. Theoretical model for the formation of ion-pairs in seawater. *Mar. Chem.* **1975**, *3* (4), 365–374.
- (46) Gómez-Morales, J.; Hernández-Hernández, A. N.; Sasaki, G.; García-Ruiz, J. M. Nucleation and Polymorphism of Calcium Carbonate by a Vapor Diffusion Sitting Drop Crystallization Technique. *Cryst. Growth Des.* **2009**, *10* (2), 963–969.
- (47) Hernández-Hernández, A.; Rodríguez-Navarro, A. B.; Gómez-Morales, J.; Jiménez-Lopez, C.; Nys, Y.; García-Ruiz, J. M. Influence of Model Globular Proteins with Different Isoelectric Points on the Precipitation of Calcium Carbonate. *Cryst. Growth Des.* **2008**, *8* (5), 1495–1502.
- (48) Kawano, J.; Shimobayashi, N.; Kitamura, M.; Shinoda, K.; Aikawa, N. Formation process of calcium carbonate from highly supersaturated solution. *J. Cryst. Growth* **2002**, *237*, 419–423.
- (49) Xin, R.; Leng, Y.; Wang, N. In situ TEM examinations of octacalcium phosphate to hydroxyapatite transformation. *J. Cryst. Growth* **2006**, *289* (1), 339–344.
- (50) Lee, I. S.; Kim, K. T.; Lee, A. Y.; Myerson, A. S. Concomitant Crystallization of Glycine on Patterned Substrates: The Effect of pH on the Polymorphic Outcome. *Cryst. Growth Des.* **2008**, *8* (1), 108–113.
- (51) Mangin, D.; Puel, F.; Veessler, S. Polymorphism in Processes of Crystallization in Solution: A Practical Review. *Org. Process Res. Dev.* **2009**, *13* (6), 1241–1253.
- (52) Lin, Y.; Singer, P. Effects of seed material and solution composition on calcite precipitation. *Geochim. Cosmochim. Acta* **2005**, *69*, 4495–4504.
- (53) Nehrke, G.; Reichart, G.; Van Cappellen, P.; Meile, C.; Bijma, J. Dependence of calcite growth rate and Sr partitioning on solution stoichiometry: non-Kossel crystal growth. *Geochim. Cosmochim. Acta* **2007**, *71*, 2240–2249.
- (54) Perdikouri, C.; Putnis, C.; Kasiotas, A.; Putnis, A. An atomic force microscopy study of the growth of a calcite surface as a function of calcium/carbonate concentration ratio in solution at constant supersaturation. *Cryst. Growth Des.* **2009**, *9* (10), 4344–4350.
- (55) Gómez-Morales, J.; Torrent-Burgués, J.; López-Macipe, A.; Rodríguez-Clemente, R. Precipitation of calcium carbonate from solutions with varying Ca²⁺ carbonate ratios. *J. Cryst. Growth* **1996**, *166* (1–4), 1020–1026.
- (56) Tai, C.; Lu, J.; Wu, J. Crystal growth rate of calcite in a constant composition environment. *J. Chin. Inst. Chem. Eng.* **2005**, *36*, 443–450.
- (57) Gebrehiwet, T.; Redden, G.; Fujita, Y.; Beig, M.; Smith, R. The Effect of the CO₃²⁻ to Ca²⁺ Ion activity ratio on calcite precipitation kinetics and Sr²⁺ partitioning. *Geochem. Trans.* **2012**, *13* (1), 1–11.
- (58) Boistelle, R.; Lopez-Valero, I. Growth units and nucleation: the case of calcium phosphates. *J. Cryst. Growth* **1990**, *102* (3), 609–617.
- (59) Stephens, C. J.; Ladden, S. F.; Meldrum, F. C.; Christenson, H. K. Amorphous Calcium Carbonate is Stabilized in Confinement. *Adv. Funct. Mater.* **2010**, *20* (13), 2108–2115.
- (60) Grossier, R.; Hammadi, Z.; Morin, R.; Veessler, S. Predictive Nucleation of Crystals in Small Volumes and Its Consequences. *Phys. Rev. Lett.* **2011**, *107* (2), No. 025504.
- (61) Howard, E. I.; Fernandez, J. M.; Garcia-Ruiz, J. M. On the Mixing of Protein Crystallization Cocktails. *Cryst. Growth Des.* **2009**, *9* (6), 2707–2712.
- (62) Bird, R.; Stewart, W.; Lightfoot, E. *Transport Phenomena*, 2nd ed.; John Wiley & Sons: New York, 2002.
- (63) Krauss, F.; Schriever, W. Die Hydrate des Calciumcarbonats. *Z. Anorg. Allg. Chem.* **1930**, *188* (1), 259–273.
- (64) Fukushi, K.; Munemoto, T.; Sakai, M.; Yagi, S. Monohydrocalcite: A promising remediation material for hazardous anions. *Sci. Technol. Adv. Mater.* **2011**, *12* (6), No. 0647021.
- (65) Yamaguchi, T.; Murakawa, K. Preparation of spherical CaCO₃ (vaterite) powder transition to calcite in water. *Zairyo* **1981**, *30*, 856–860.
- (66) Taft, W. H. Chapter 3: Physical Chemistry of Formation of Carbonates. In *Developments in Sedimentology*; George, V., Chilingar, H. J. B., Rhodes, W. F., Eds.; Elsevier: Amsterdam, 1967; Vol. 9, Part B, pp 151–167.
- (67) Ogino, T.; Suzuki, T.; Sawada, K. The rate and mechanism of polymorphic transformation of calcium carbonate in water. *J. Cryst. Growth* **1990**, *100* (1–2), 159–167.
- (68) Ildefonso, M.; Revalor, E.; Punniyam, P.; Salmon, J. B.; Candoni, N.; Veessler, S. Nucleation and polymorphism explored via an easy-to-use microfluidic tool. *J. Cryst. Growth* **2012**, *342* (1), 9–12.
- (69) Hammadi, Z.; Candoni, N.; Grossier, R.; Ildefonso, M.; Morin, R.; Veessler, S. Small-volume nucleation. *C. R. Phys.* **2013**, *14* (2–3), 192–198.